

**ICSO 2016**

**International Conference on Space Optics**

Biarritz, France

18–21 October 2016

*Edited by Bruno Cugny, Nikos Karafolas and Zoran Sodnik*



***Laser module based on monolithically integrated Mopas at 1.5  $\mu\text{m}$  for space-borne lidar applications***

*M. Faugeron*

*S. Klein*

*M. Villera*

*G. Kochem*

*et al.*



## LASER MODULE BASED ON MONOLITHICALLY INTEGRATED MOPAS AT 1.5 $\mu\text{M}$ FOR SPACE-BORNE LIDAR APPLICATIONS

M. Faugeron<sup>1,\*</sup>, S. Klein<sup>2</sup>, M. Vilera<sup>3</sup>, G. Kochem<sup>2</sup>, A. Pérez-Serrano<sup>3</sup>, M. Krakowski<sup>1</sup>, M. Traub<sup>2</sup>,  
F. van Dijk<sup>1</sup> and I. Esquivias<sup>3</sup>

<sup>1</sup> III-V Lab Campus Polytechnique, Palaiseau, France. \* now with Thales Alenia Space, Toulouse, France.

<sup>2</sup> Fraunhofer Institute for Laser Technology ILT, Aachen, Germany. <sup>3</sup> CEMDATIC-ETSI Telecomunicación, Universidad Politécnica de Madrid, Spain.

### I. INTRODUCTION

Space-borne lidar systems require laser transmitters with very good performance in terms of output power, beam quality, conversion efficiency, long term reliability and environmental compatibility. Atmospheric gas sensing additionally requires spectral purity and stability. Solid state lasers are considered the most mature technology for space lidar applications, at expenses of a relatively large size and low conversion efficiency [1]-[3]. Fiber lasers present very high power levels and very good beam quality, but they require specific attention due to their sensitivity to radiation. In this sense, progresses have been made to develop high power fiber amplifiers for different space applications [4]-[6]. Recently, a new generation of high brightness semiconductor lasers based on tapered geometry has demonstrated relatively high average power levels together with a good beam quality [7]-[10]. These devices are emerging candidates for its direct use in space lidar systems.

Semiconductor lasers have clear advantages over other laser types in terms of compactness and conversion efficiency (up to 75%). They present high reliability and good radiation hardness for most space applications. They can be fabricated with emission wavelengths ranging from Ultra-Violet up to Far-Infrared, and those with appropriate design can be tuned over several tenths of nanometers. Broad Area lasers can achieve more than 20 W CW, but they suffer from a poor beam quality. Tapered semiconductor lasers [7], [8], also known as flared unstable cavity lasers, have demonstrated both high power and good beam quality at different wavelengths. These devices consist of a ridge waveguide (RW) section and a tapered section. The single spatial mode of the RW section is launched into the tapered section where it is amplified while keeping its single mode profile. Improved epitaxial structures, together with the use of long cavity designs have led to single-emitter tapered lasers providing more than 10 W with a low beam propagation ratio  $M^2$  at 980 nm [8] and 1060 nm [7]. The spectral properties of tapered lasers are similar to those of BA lasers, with multiple modes and broad and unstable emission spectra, but they can be enhanced by the use of a Distributed Bragg Reflector (DBR) to select a single longitudinal mode [8]. The integrated Master Oscillator Power Amplifier (MOPA) architecture, consisting of either a Distributed Feedback (DFB) or a DBR laser as oscillator and a tapered semiconductor amplifier, present advantages for those lidar applications requiring good spectral properties. Integrated DBR MOPAs have demonstrated up to 12 W in CW operation and 42 W in pulsed operation at 1064 nm [9]. DFB-based MOPAs are commercially available at different wavelengths, and have reached 1.6 W in CW operation and 2.7 W in pulsed operation at eye-safe wavelengths, around 1500 nm [10].

Most of lidar systems are based in high peak power pulses with a low repetition rate, but the maximum peak power of semiconductor lasers is quite limited in comparison with solid state or fiber lasers. Intensity modulated CW (IM-CW) lidar systems are more appropriate to take advantage of the modulation properties of these devices. Random-modulation CW (RM-CW) lidar [11] is capable of obtaining range gated back-scattering information as obtained from pulsed techniques.

In the framework of the European Project BRITESPACE [12] we investigated on a RM-CW Integrated Path Differential Absorption (IPDA) lidar for column-averaged measurements of atmospheric CO<sub>2</sub> to be used in future space missions [13]. Fig. 1 shows the schematics of the proposed RM-CW IPDA lidar system. At its core, two integrated three-section MOPAs emitting at 1572 nm are used [14]. These are thermally controlled via Thermoelectric Coolers (TECs). An optical-electrical feedback loop, the so-called Frequency Stabilization Unit (FSU) based on a gas cell reference is used in each laser chip in order to have highly stable emission frequencies and narrow linewidths. Both wavelength signals are transmitted through two telescopes. The modulation bit rate is set to 25 Mb/s (clock period of 40 ns), which provides a distance resolution of 6 m. The backscattered light (the received on- and off-line channels) is collected by a reflective telescope with a field-of-view slightly greater than the laser beam divergence. The collimated light is focused onto a single photon detector, a Negative Feedback Avalanche Diode (NFAD). The measurement of the Differential Absorption Optical Depth (DAOD), related to the CO<sub>2</sub> concentration, involves not only the on- and off-line energy of the received channels but also the accurate measurement of the emitted energy via the transmission channels. Such measurements are taken from sampling the transmitted beams via mirror back-leakage and an integrating sphere (for the purpose of homogenizing and attenuation). In addition, a rotational diffuser is used to minimize the speckle noise in the references. A short wave infrared (SWIR) camera is used for aligning the emitted and received spots to the detector. At the single photon

detector, incident photons trigger an avalanche event, which outputs an electrical pulse. These pulses are then cross-correlated with the transmitted random code resulting in range resolved returns that are equivalent to those obtained in a backscattered pulsed system. The original random code and cross-correlation are realized by means of a Field Programmable Gate Array (FPGA).

The theoretical details on the space-borne implementation of such a RM-CW IPDA lidar system can be found in [15]. The parameter study has revealed that a worst case retrieval precision of 1.5 ppm over a 50 km path integration can be obtained assuming state-of-the-art single photon counting detectors and transmitters delivering an average power of 2 W. On the other hand, the RM-CW IPDA system approach has been validated using DFBs lasers modulated with Acousto-Optic Modulators (AOM) and amplification by an Erbium Doped Fiber Amplifier (EDFA) [16]. The experimental results obtained in a 3 km horizontal path show a precision of 2.5 ppm for 7 s integration with an average output power of 300 mW for each sounding frequency.

In this contribution, we present the design, fabrication and experimental results of the laser transmitter module prototype for the RM-CW IPDA lidar system. The paper is organized as follows. In Section II, a summary of the design and characteristics of the three-section MOPAs devices is given. In Section III, the design and fabrication of the laser modules is detailed. In Section IV, the experimental results obtained from the laser module operation are shown. Special emphasis is given to the beam quality and modulation characteristics. Finally, the conclusions are drawn in Section V.

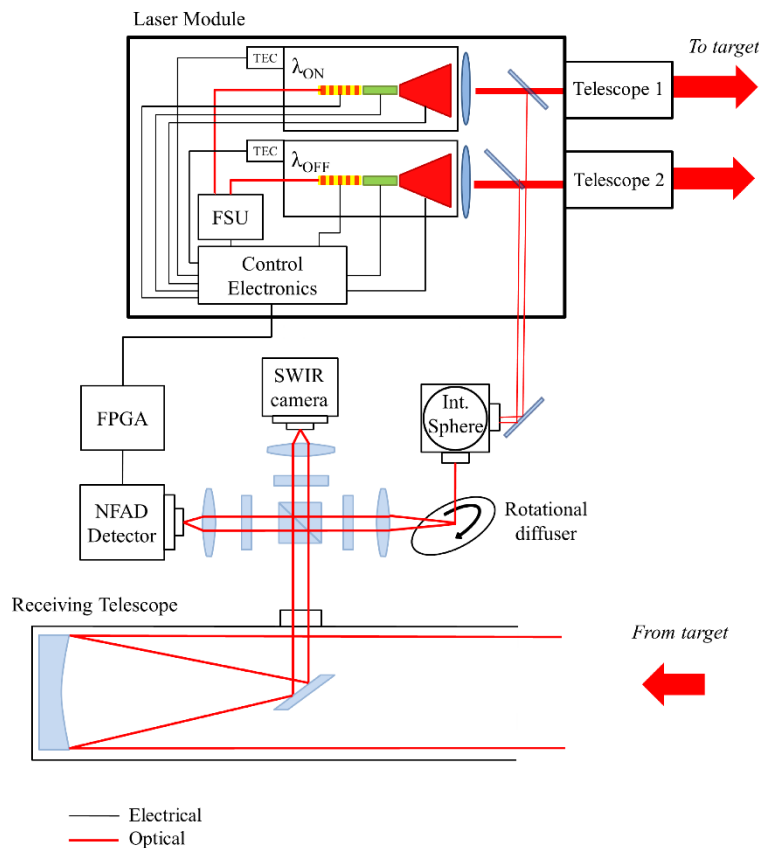


**Fig. 1.** Schematics of the proposed RM-CW IPDA lidar instrument. FSU: Frequency Stabilization Unit. SWIR: Short-Wave Infra-Red. NFAD: Negative Feedback Avalanche Diode. FPGA: Field Programmable Gate Array.

## II. THREE-SECTION MONOLITHIC MASTER OSCILLATOR POWER AMPLIFIER

InGaAsP/InP monolithic MOPAs were fabricated as the main building block of the laser transmitter. Each MOPA is a three section device, consisting of a frequency stabilized DFB master oscillator, a modulator section, and a tapered Semiconductor Optical Amplifier (SOA). The use of this original structure aims to fulfill the performances required by the IPDA system in terms of high power, frequency stability and good beam quality. The DFB section is accurately frequency stabilized by an external opto-electrical feedback loop through the FSU. The modulator section is introduced for implementation of the RM-CW technique in the proposed IPDA system.

Finally, the geometry of the tapered SOA is optimized in order to provide high brightness output beam with sufficient power and beam quality.

We have designed our asymmetrical cladding structure using a dilute slab composed of InP and InGaAsP ( $\lambda_g = 1.17 \mu\text{m}$ ) in order to avoid any material development. This quaternary material is the same as the barrier material. The slab thickness ( $1.62 \mu\text{m}$ ) has been optimized to decrease the optical confinement within the p-doped layers as much as possible and to maintain the confinement within the Quantum Wells (QWs) around 2%. This level of confinement is necessary to maintain a low threshold current, a low RIN and a quite large relaxation frequency.

The multiple QWs DFB structure was grown by Metal Organic Chemical Vapor Deposition (MOCVD) on n-InP substrates. The active region contains six 8 nm thick compressively (0.85%) strained InGaAsP quantum wells and five 10 nm thick InGaAsP ( $\lambda_g = 1.17 \mu\text{m}$ ) barriers. The photoluminescence peak was  $1.57 \mu\text{m}$ . After a first epitaxy, first order gratings were defined by e-beam lithography and inductively coupled plasma (ICP) reactive ion etching. The InGaAsP grating layer is positioned above the active zone and the grating layer thickness is optimized in order to obtain a coupling strength  $\kappa L \sim 1.4$ . This low value of  $\kappa L$  should limit spatial hole burning and the associated optical power saturation. Re-growth of p-doped top cladding was then also done by MOCVD. The ridge-waveguides are  $3.0 \mu\text{m}$  wide. This value was found to minimize the thermal saturation while preserving lateral single-mode operation. Bars were cleaved to form 4 and 5 mm long devices. Facets were high reflectivity (HR) coated on the DFB laser backside facet and antireflection (AR) coated on the SOA facet. Chips cleaved from the bars were mounted p-side up on aluminum nitride (AlN) sub-mounts. A thermistor was glued on the sub-mount to better control the chip temperature.

Standard straight monolithically integrated MOPAs exhibit instabilities due to compound cavity effects arising from the residual reflectivity at the amplifier output facet [17, 18]. In order to decrease the reflections at the facets, a simple method consists in tilting the device with regard to the facets. This technique is very common for SOAs. The main drawback is the difficulty to make efficient high reflective coatings on the backside DFB laser facet due to the tilt. This problem has been solved by using a bent structure as shown in Fig. 2 (a). A photograph of the devices is shown in Fig. 2 (b). For this particular device, we observe stable emission around  $1583 \text{ nm}$  with a side mode suppression ratio better than 45 dB. Other devices from other fabrication runs have achieved the target frequency of  $1572 \text{ nm}$ . Fig. 2 (c) shows the optical power as a function of the amplifier current  $I_{PA}$  ( $I_{DFB} = 0.4$ ,  $I_{MOD} = 300 \text{ mA}$ ). The maximum optical power is  $420 \text{ mW}$  at  $18^\circ\text{C}$  ( $I_{PA} = 3 \text{ A}$ ); by decreasing the temperature to  $12$  and  $6^\circ\text{C}$ , we have obtained a maximum output power of  $510$  and  $600 \text{ mW}$  respectively. Fig. 2 (d) shows the optical spectra dependence on  $I_{DFB}$  for  $I_{MOD} = 300 \text{ mA}$  and  $I_{PA} = 3 \text{ A}$ . The laser exhibits multimode operation close to the threshold (DFB laser without phase-shift) and single-mode operation without any mode hopping from  $300$  to  $500 \text{ mA}$ .

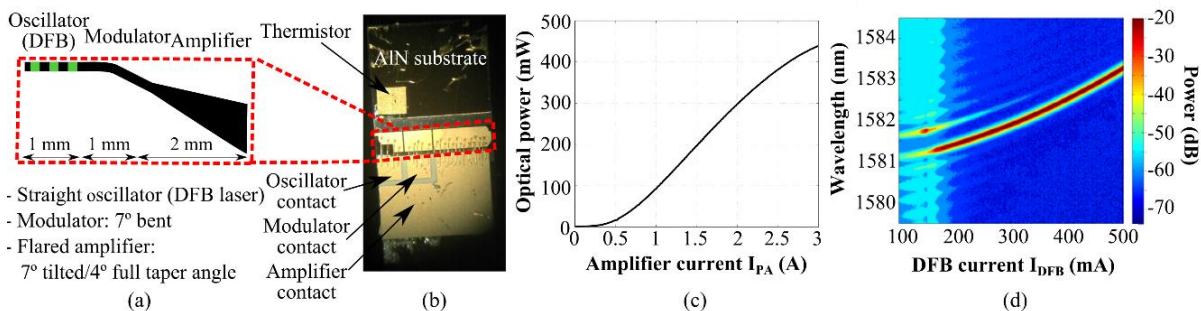


**Fig. 2.** Fabricated three-section bent MOPAs. (a) Schematics of the device. (b) Photograph of the device. (c) Power vs PA current characteristics at  $T = 18^\circ\text{C}$ . (d) Optical spectrum while varying the DFB current.

### III. LASER MODULE

The CAD design of the laser module and the subsequently fabricated module are shown in Fig. 3. It is intended as a proof-of-concept and to be used in various free space and laboratory tests. For this reason the design focusses more on accessibility to the different parts of the transmitter and versatility rather than space compatibility and compactness. The module uses two MOPAs as beam sources. They are mounted on copper heatsinks, which are temperature controlled by TECs. The temperature in each heatsink is monitored with a thermistor and the waste heat of the TECs is dissipated via water cooling. The beam emitted from the tapered section of the MOPAs is astigmatic (i.e. has different source points in the slow and fast axis; see Fig. 4 a). Therefore two lenses are used to collimate it, in this case an aspherical fast-axis collimation (FAC) lens and a cylindrical slow-axis collimation (SAC) lens (see Fig. 4 b). A small amount of power is also emitted from the back facet of the DFB section, which is coupled in a single mode fiber (SMF), to be used in the FSU. In the realized module a collimation lens and a

focusing lens were used to realize the SMF coupling (see Fig 4 b). Coupling into a lensed fiber was also tried, but proved to be unstable and difficult to align due to the relatively low optical power available from the back facet.

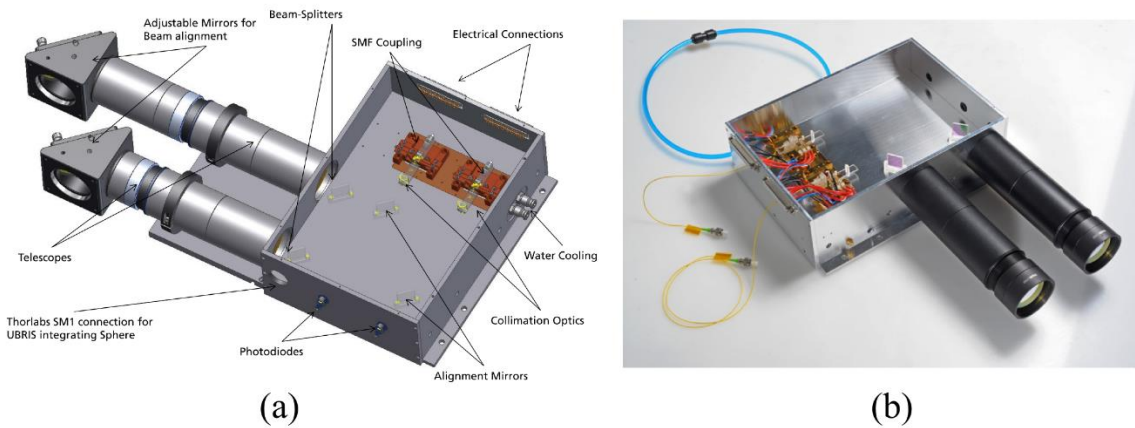


**Fig. 3.** Laser transmitter module. (a) CAD design. (b) Photograph of the fabricated device.

The performance of the collimation optics is shown in Fig. 5 using the wavefront map and the spot diagram. A single MOPA mounted on its heatsink with collimation optics, SMF coupling and electrical connectors is shown in Fig. 6.

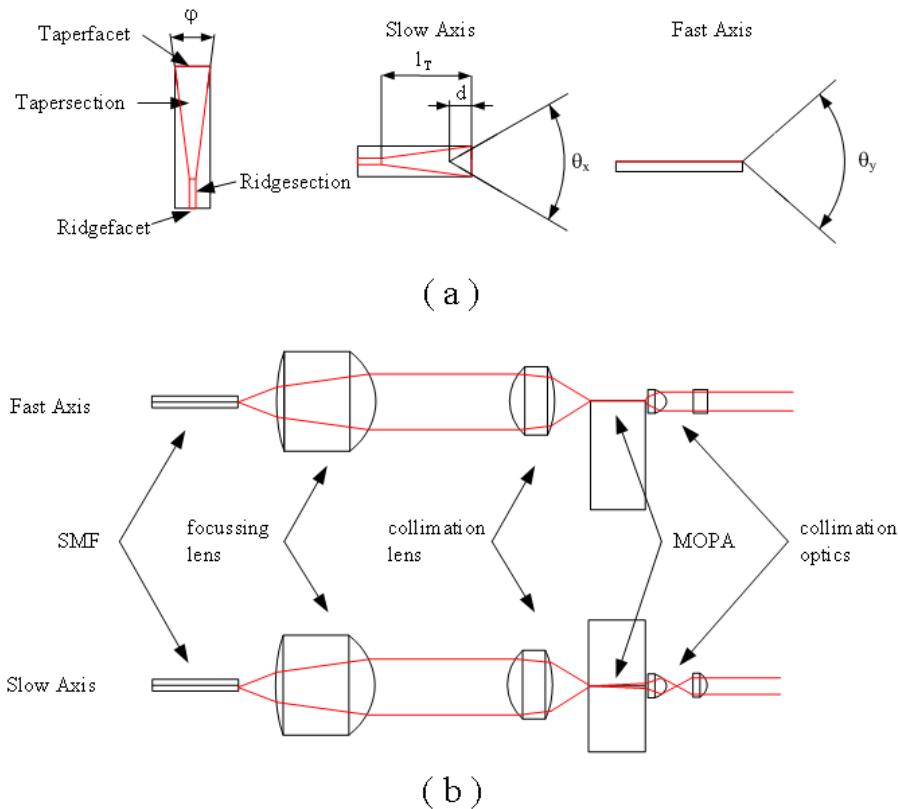


**Fig. 4.** (a) Astigmatic beam emitted by tapered amplifier. (b) Optical system - collimation and SMF coupling.

The collimated beams are aligned to the telescopes using mirrors, and small fractions of the optical power are redirected to photo diodes for monitoring purposes and to an integrating sphere as a reference signal. An additional set of adjustable mirrors can be mounted on the telescopes to aim the two beams and thus minimizing footprint errors in IPDA detection. Connectors for the water cooling, the temperature control and the power supply for the MOPAs are integrated in the module housing (see Fig. 3).

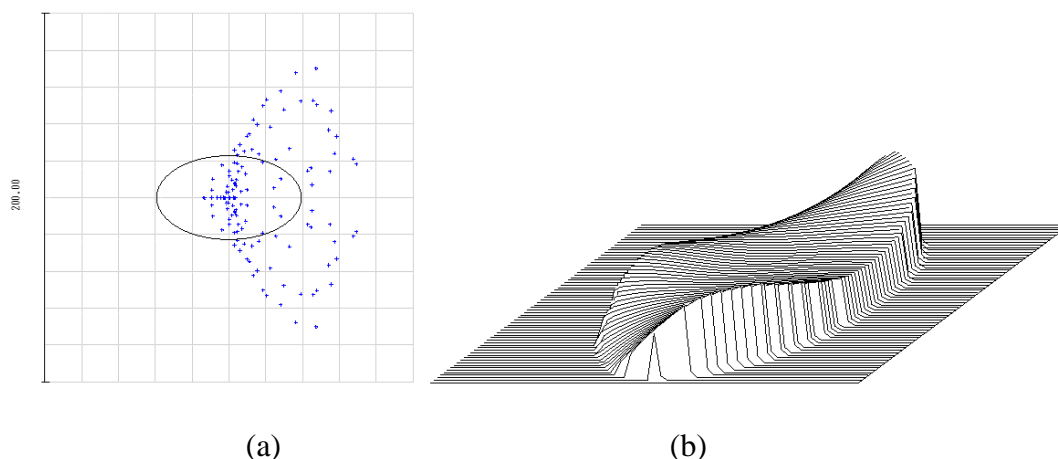


**Fig. 5:** Performance of collimation optics: (a) Spot diagram (with airy disc). (b) Wavefront map (peak to valley: 0.9861 waves)

The optical-optical efficiency of the beam forming optics was measured to be above 90%. The divergence angle in the collimated beam before the telescopes amounts to 1.3 mrad in fast and 2.3 mrad in slow axis. With a magnification factor of 11 in the telescope, this leads to a final value of 120  $\mu$ rad for the fast and 210  $\mu$ rad for the slow axis. The best coupling efficiency achieved in SMF on the back facet was 68% (2.4 mW coupled in the SMF out of 3.8 mW emitted from the back facet). This was reduced to ~50% in the realized module due to adhesive shrinkage.

The presented module is not suitable for space applications, mostly due to its size and weight and the use of water cooling. However, as a proof of concept, a sub-module containing only one MOPA and the necessary optics and interfaces was designed and fabricated, which weighed 200g and had dimensions of 57x79.7x27 mm<sup>3</sup>.

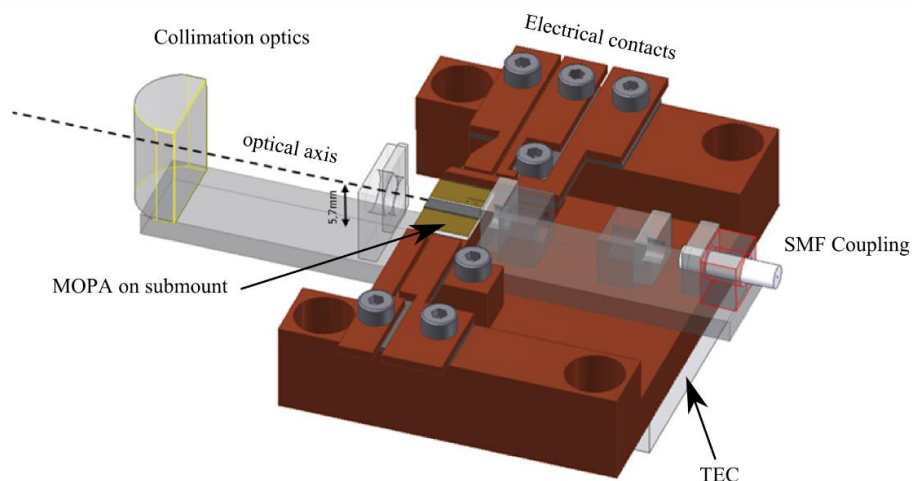


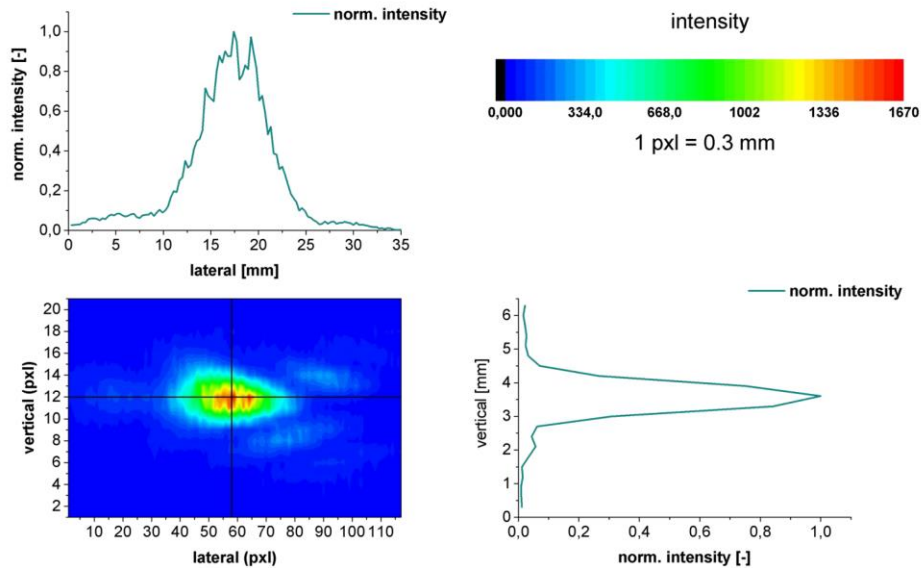
**Fig. 6.** MOPA mount with collimation optics and backside SMF coupling.

#### IV. EXPERIMENTAL RESULTS

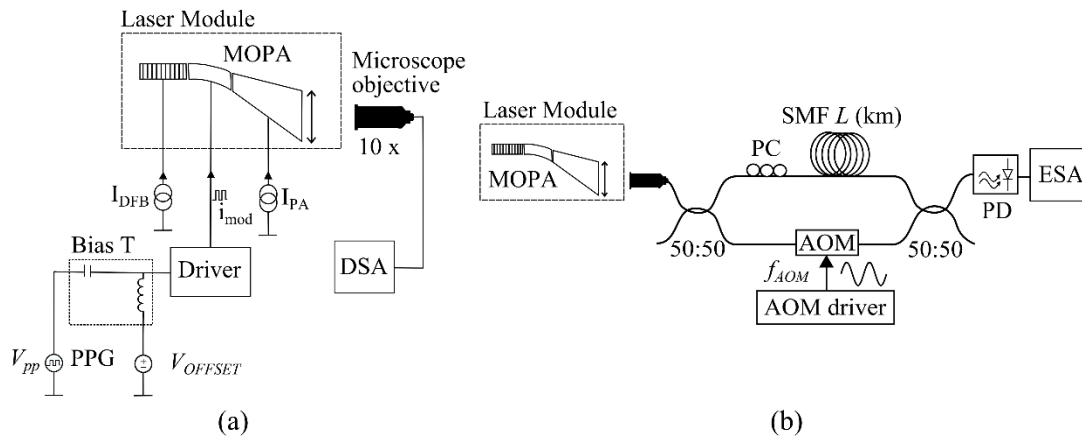
The best results in the collimation of the output beam were obtained using a spherical FAC lens (Thorlabs 355392) and a cylindrical SAC lens (Thorlabs Lj1878L1). Fig. 7 shows the far field of the slow (lateral) and fast (vertical) axes are shown. The measured slow axis beam propagation factor  $M^2$  was 2.65.

In order to modulate the laser module, an in-house driver was developed. Fig. 8(a) illustrates the experimental setup to characterize the performance under intensity modulation of the modulator section. A CW current,  $I_{DFB}$ , drives the DFB section;  $i_{mod}$  is the result of the superposition of two signals in the driver: a CW current,  $I_{MOD}$ , and a squared wave provided by a Pulse Pattern Generator (PPG) (Anritsu MU181020A) at a variable frequency  $f_{clock}$  and with maximum peak to peak voltage  $V_{pp} = 2.5$  V. The measurements were performed using an optical input channel of a Digital Serial Analyzer (DSA) sampling oscilloscope (Tektronix DSA8200). The nonlinear behavior

of the devices makes difficult to estimate the real voltage or current applied to them; we use as reference  $V_{pp}$  which refers to the voltage applied by the PPG to an ideal  $50 \Omega$  load. Finally, a CW current source supplies  $I_{PA}$  to the amplifier section.

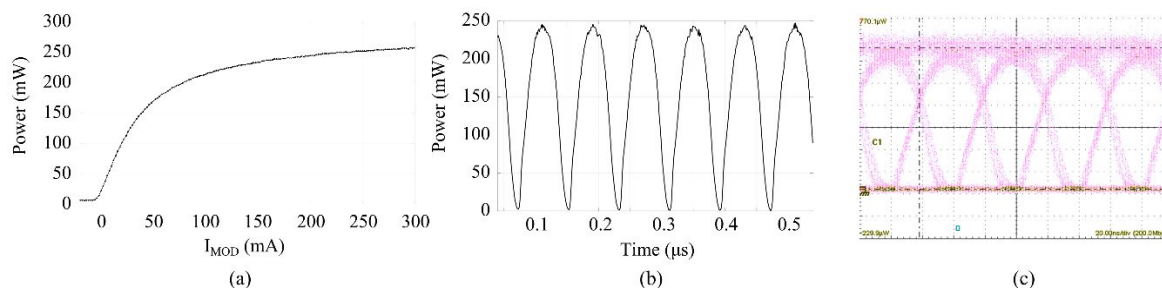


**Fig. 7.** Far field measurement. The collimation optics were formed using a spherical FAC lens and a cylindrical SAC lens.  $I_{DFB} = 400$  mA,  $I_{MOD} = 300$  mA and  $I_{PA} = 3$  A.  $M^2 = 2.65$ .



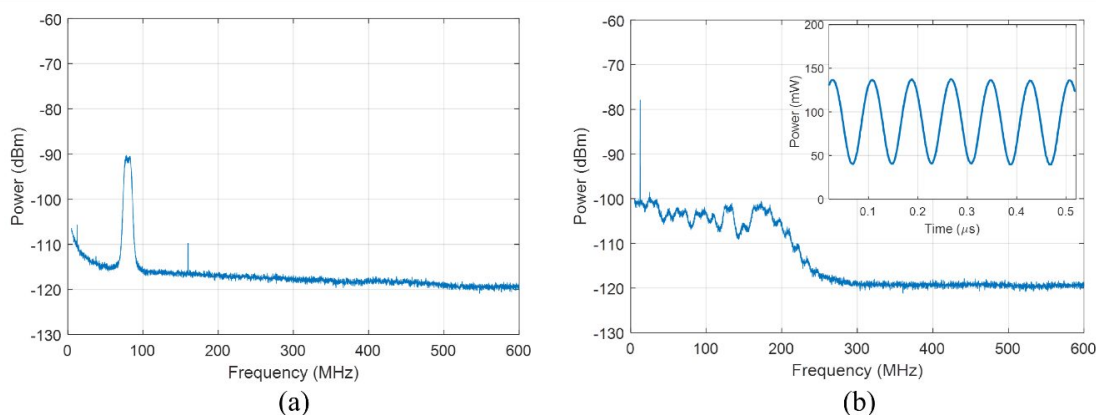
**Fig. 8.** (a) Module modulation setup using an in-house driver and the three-section MOPA packaged in the laser module. (b) Self-heterodyne setup used for measuring the emission linewidth and the impact of the modulation on the spectrum.

Fig. 9 (a) shows the power- $I_{MOD}$  characteristics of the laser module, while maintaining constant  $I_{DFB}$  and  $I_{PA}$ . The power was measured with a thermal detector (Gentec UP19K-30H-H5) placed in the collimated output beam. The dimensions of the MOPA mounted in the module were 1.5 mm, 1 mm and 2.5 mm for the DFB, modulator and amplifier sections, respectively. This measurement and those reported below were performed at heat-sink temperature of  $15^\circ\text{C}$ . The maximum power out of the module for this device was around 250 mW. As it can be observed in Fig 9 (a) the modulator section acts as an absorber, decreasing the output power when negative current is applied, or as an amplifier when driven at positive bias. Fig. 9 (b) and (c) shows the modulation results for a square excitation at the application frequency of 12.5 MHz. Fig. 9 (b) shows a time trace obtained with the DSA. Although the squared shape has been smoothed, the high and low levels can be clearly distinguished. Fig. 9 (c) shows the measured eye-diagram using a pseudo random bit sequence non return to zero at 25 Mb/s of 252 bits. A Quality factor  $Q = 12$  and an Extinction Ratio (ER) = 24.2 dB was obtained. The optical spectra under modulation were measured with an Optical Spectrum Analyzer (ANDO AQ6315A) with a resolution of 6.25 GHz not showing spectral broadening within this resolution range.



**Fig. 9.** (a) Power-current characteristics.  $I_{DFB} = 500$  mA and  $I_{PA} = 3.5$  A. (b) Modulation results for a square function at the application frequency of 12.5 MHz. Time trace obtained. (c) Eye diagram showing a  $Q = 12$ , eye height = 154 mW and  $I_{DFB} = 500$  mA,  $I_{PA} = 3.5$  A,  $V_{OFFSET} = 0.67$  V,  $V_{pp} = 800$  mV.

In order to further characterize the impact of the modulation in emission spectrum, we use the optical self-heterodyne setup [19] shown in Fig. 8 (b). A fraction of the collimated beam is coupled into a SMF, and then the light is split in two paths to be combined later in a second coupler and applied to a photodiode. On the upper path, the optical signal is delayed respect the lower by using a 5 km long SMF with the goal of providing an incoherent beating between both signals. In the lower path, an AOM shifts the optical frequency 80 MHz, and thus the beating tone after the photodiode is centered at 80 MHz. Fig. 10 (a) shows the RF spectrum measured in the photodiode with an Electrical Signal Analyzer (Agilent E4446A) with the laser module driven in CW operation. The peak at 80 MHz has a Gaussian shape and the corresponding optical emission linewidth is around 5 MHz. Fig. 10 (b) shows the RF spectrum in the photodiode when the laser module was driven under sinusoidal modulation at 12.5 MHz. The inset of Fig. 10 (b) shows the output power with optical modulation amplitude of around 100 mW. The RF spectrum shows clear features of frequency modulation, attributed to the variation of the modulator refractive index when changing the current and therefore the carrier concentration. The absence of the carrier peak at 80 MHz and the sequence of amplitudes in the harmonics values correspond to a composition of Bessel functions of first order. The broadening of the spectra depends on the modulation depth and on the bias level. A detailed analysis of the spectral broadening will be reported with more detail elsewhere.



**Fig. 10.** RF spectra measured in the self-heterodyne set up in the following conditions: (a) CW operation;  $I_{DFB} = 430$  mA,  $I_{MOD} = 25$  mA and  $I_{PA} = 3.5$  A. (b) Sinusoidal modulation at 12.5 MHz;  $I_{DFB} = 430$  mA,  $I_{PA} = 3.5$  A,  $I_{MOD} = 25$  mA and  $V_{pp} = 800$  mV. Inset: Time trace.

## VI. CONCLUSIONS

We have shown that semiconductor lasers, in particular the fabricated three-section integrated MOPA devices, are promising candidates for future implementation in space-borne IPDA lidar systems for atmospheric  $CO_2$  measurements. We have reported on the fabrication and the peculiarities of the three-section MOPA devices. These characteristics have to be taken into account in order to fabricate the appropriate laser transmitter module. We have found that in order to get the best beam quality, one spherical FAC lens and one cylindrical SAC lens are the best choices for the output beam collimation. Obtaining a beam quality factor of  $M^2 = 2.65$ .

On the modulation characteristics, we have shown that the laser module can be modulated at the frequency required by the application (12.5 MHz) obtaining a very good and clearly open eye diagram. Regarding the impact of the modulation over the emission spectrum, we have found evidences of frequency modulation. The impact of

the effect of frequency modulation in the RM-CW IPDA lidar application should be addressed and will be the subject of further investigation.

#### ACKNOWLEDGMENT

This work was supported by the European Commission through the project FP7-SPACE BRITESPACE under grant agreement no. 313200. A. Pérez-Serrano and I. Esquivias also acknowledge support from the Ministerio de Economía y Competitividad of Spain under projects RANGER (TEC2012-38864-C03-02) and COMBINA (TEC2015-65212-C3-2-P); and the Comunidad de Madrid under program SINFOTON-CM (S2013/MIT-2790). A. Pérez-Serrano acknowledges support from Ayudas a la Formación Posdoctoral 2013 program (FPDI-2013-15740).

#### REFERENCES

- [1] R. A. Robinson, T. D. Gardiner, F. Innocenti, A. Finlayson, P. T. Woods, and J. F. M. Few, "First measurements of a carbon dioxide plume from an industrial source using a ground based mobile differential absorption lidar," *Environ. Sci.: Processes Impacts* vol. 16, pp. 1957-1966, 2014.
- [2] T. F. Refaat, U. N. Singh, J. Yu, M. Petros, S. Ismail, M. J. Kavaya, and K.J. Davis, "Evaluation of an airborne triple-pulsed 2  $\mu\text{m}$  IPDA lidar for simultaneous and independent atmospheric water vapor and carbon dioxide measurements," *Appl. Opt.*, vol. 54, pp. 1387-1398, 2015.
- [3] F. Gibert, D. Edouart, and C. Cénac, "2- $\mu\text{m}$  high-power multiple frequency single-mode Q-switched Ho:YLF laser for DIAL application," *Appl. Phys. B*, vol. 116, pp. 967-976, 2014.
- [4] A. W. Yu, J. B. Abshire, M. Storm, and A. Betin, "Laser amplifier development for IPDA Lidar measurements of CO<sub>2</sub> from space." *Proc. SPIE*, vol. 9342, Solid State Lasers XXIV: Technology and Devices, 93420M, 2015.
- [5] S. Gupta, *et al.*, "Development, testing, and initial space qualification of 1.5- $\mu\text{m}$ , high-power (6 w), pulse-position-modulated fiber laser transmitter for deep-space laser communication." *Opt. Eng.*, vol. 55, no. 11, p. 111606, 2016.
- [6] M. Storm, D. Engin, B. Mathason, R. Utano, and S. Gupta, "Space-Based Erbium-Doped Fiber Amplifier Transmitters for Coherent, Ranging, 3D-Imaging, Altimetry, Topology, and Carbon Dioxide Lidar and Earth and Planetary Optical Laser Communications," *EPJ Web of Conferences*, vol. 119, p. 02002, 2016.
- [7] B. Sumpf, *et al.*, "High-Brightness Quantum Well Tapered Lasers," *IEEE J. Selected Topics Quantum Electron.*, vol. 15, pp. 1009-1020, 2009.
- [8] C. Fiebig, *et al.*, "High-Power DBR-Tapered Laser at 980 nm for Single-Path Second Harmonic Generation," *IEEE J. Select. Topics Quantum Electron.* vol. 15, pp. 978-983, 2009.
- [9] H. Wenzel, *et al.*, "High peak power optical pulses generated with a monolithic master-oscillator power amplifier," *Opt. Lett.*, vol. 37, pp. 1826-1828, 2012.
- [10] P. Adamiec, B. Bonilla, A. Consoli, J. M. G. Tijero, S. Aguilera, and I. Esquivias, "High-peak-power pulse generation from a monolithic master oscillator power amplifier at 1.5  $\mu\text{m}$ ," *Appl. Opt.*, vol. 51, pp. 7160-7164, 2012.
- [11] N. Takeuchi, N. Sugimoto, H. Baba, and K. Sakurai, "Random modulation cw lidar," *Appl. Opt.*, vol. 22, pp. 1382-1386, 1983.
- [12] [www.britespace.eu](http://www.britespace.eu)
- [13] G. Ehret, C. Kiemle, M. Wirth, A. Amediek, A. Fix, and S. Houweling, "Space-borne remote sensing of CO<sub>2</sub>, CH<sub>4</sub>, and N<sub>2</sub>O by integrated path differential absorption lidar: A sensitivity analysis," *Appl. Phys. B*, vol. 90, pp. 593-608, 2008.
- [14] M. Faugeron, *et al.*, "High power three-section integrated master oscillator power amplifier at 1.5  $\mu\text{m}$ ," *IEEE Photon. Technol. Lett.*, vol. 27, pp. 1449-1452, 2015.
- [15] X. Ai, *et al.*, "Analysis of a random modulation single photon counting differential absorption lidar system for space-borne atmospheric CO<sub>2</sub> sensing," *Opt. Express*, vol. 24, no. 18, pp. 21119-21133, 2016.
- [16] M. Quatrevalet, *et al.*, "Atmospheric CO<sub>2</sub> Sensing with a Random Modulation Continuous Wave Integrated Path Differential Absorption Lidar", submitted.
- [17] M. Spreemann, M. Lichtner, M. Radziunas, U. Bandelow, and H. Wenzel, "Measurement and simulation of distributed feedback tapered master-oscillator power-amplifiers" *IEEE J. Quantum Electron.*, vol. 45, pp. 609-616, 2009.
- [18] M. Vilera, A. Pérez-Serrano, J.M.G. Tijero and I. Esquivias, "Emission Characteristics of a 1.5  $\mu\text{m}$  All Semiconductor Tapered Master Oscillator Power Amplifier", *IEEE Photon. J.*, vol. 7, no. 2, p. 1500709, 2015.
- [19] T. Okoshi, K. Kikuchi, and A. Nakayama, "Novel method for high resolution measurement of laser output spectrum," *Electron. Lett.*, vol. 16, pp. 630-631, 1980.